Available online at www.CivileJournal.org

Civil Engineering Journal

(E-ISSN: 2476-3055; ISSN: 2676-6957)

Vol. 11, No. 08, August, 2025

Analysis of GNSS-IMU Lidar Integration for Indoor Positioning Using Unscented Kalman Filter

Qarina Putri Amelia Nuri Ila [1], Mokhamad N. Cahyadi [1, 2*], Tahiyatul Asfihani [3], Hendy F. Suhandri [4], Fadlilatul Taufany [2, 5]

[1] *Department of Geomatics Engineering, Institut Teknologi Sepuluh Nopember, Surabaya 60111, Indonesia.*

[2] *Research Center of Marine and Earth Science Technology, Directorate of Research and Community Service, Institut Teknologi Sepuluh Nopember, Surabaya 60111, Indonesia.*

[3] *Department of Mathematics, Institut Teknologi Sepuluh Nopember, Surabaya 60111, Indonesia.*

[4] *Centre of Studies for Surveying Science & Geomatics, Universiti Teknologi Mara (UiTM), Shah Alam 40450, Malaysia.*

[5] *Department of Chemical Engineering, Institut Teknologi Sepuluh Nopember, Surabaya 60111, Indonesia.*

Received 21 November 2024; Revised 11 July 2025; Accepted 17 July 2025; Published 01 August 2025

Abstract

Accurate navigation systems are important in various vehicle applications, both indoors and outdoors. Global Navigation Satellite System (GNSS) and Inertial Measurement Unit (IMU) are sensors that are often used in vehicle navigation systems. GNSS has the advantage of providing accurate position and speed information, IMU is able to make measurements without being affected by environmental conditions, and LiDAR sensors can model the environment; however, the limited signal on GNSS in indoor environments results in decreased position accuracy. The development of GNSS-IMU integration has been widely carried out, one of which is by adding a LiDAR sensor. In this study, an improvement will be made to the integration algorithm on Vision RTK2, which produces GNSS-IMU coordinate data, and Backpack Lidar, which can display 3D visualization on the traversed path using the Unscented Kalman Filter (UKF) method to improve navigation accuracy, especially in indoor environments. The results of the study showed that the UKF simulation and free outage conditions showed high accuracy with RMSE of 0.00308 m and 0.00175 m for the Easting and Northing positions and MAE of 0.00088 m and 0.00024 m. However, in outage conditions, the RMSE values were 4.0881 m and 8.6317 m, and MAE of 5.9871 m and 7.4182 m. The results of the 3D point cloud of the LiDAR model that had been georeferenced using the UKF fusion results and the KKH calculation results were validated using a rolling meter. Validation of point cloud processing from the 3D LiDAR model using a rolling meter and georeferencing with KKH calculations showed a small RMSE value, which was 0.3420 m, and 0.0354 m for the distance dimension with a rolling meter. 0.6358 m for georeferenced RMSE using UKF fusion data, and 0.0779 for distance dimension using roll meters. The small RMSE results indicate a high level of agreement between point cloud data and measurements using a rolling meter used as reference data. This study shows that the integration of GNSS-IMU sensors with LiDAR using the UKF method can improve the accuracy and reliability of indoor navigation systems.

Keywords: Backpack LiDAR; Kalman Filter; Fusi GNSS/IMU; Model 3D; Indoor Positioning.

1. Introduction

The development of indoor navigation technology has advanced rapidly in recent years. This progress has been driven by the growing demand for accurate and reliable navigation systems, both outdoors and indoors, such as in industrial buildings, office complexes, and shopping malls [1]. Although Global Navigation Satellite Systems (GNSS)

* Corresponding author: cahyadi@geodesy.its.ac.id

http://dx.doi.org/10.28991/CEJ-2025-011-08-06

can provide accurate absolute positioning over long periods, their performance is often affected by signal interference, equipment limitations, and environmental factors such as atmospheric bias and multipath effects [2-4]. One of the main challenges faced in urban or densely populated environments is GNSS Signal Outage, where the system is unable to connect to at least four satellites, resulting in reduced accuracy. This problem often occurs in areas with tall buildings, under bridges, or locations surrounded by dense trees.

Many studies have been conducted to address this challenge, one of which is by integrating GNSS with Inertial Measurement Units (IMU). The fusion of GNSS and IMU systems is an effective solution to improve position accuracy in environments with GNSS signal interference. Data fusion using the Unscented Kalman Filter (UKF) has been shown to significantly enhance position accuracy, especially in autonomous vehicles [5-7]. Additionally, the integration of LiDAR (Light Detection and Ranging) into navigation systems has made a significant contribution to generating highly accurate 3D point clouds, which are essential for indoor mapping and modeling [8].

Although many studies have been conducted to improve the accuracy of navigation systems using various Kalman filter techniques, most of these studies focus more on outdoor applications. Mousazadeh [9] used the Extended Kalman Filter (EKF) with GNSS and IMU sensors for agricultural autonomous vehicles, and Strandberg et al. [10] used UKF for sea surface height estimation using GNSS-R data. Meanwhile, Kaczmarek et al. [11] used EKF for 2D position estimation with GNSS, IMU, and odometer sensors but did not include the vertical dimension (Z/elevation). These studies generally focus on simpler position measurements and have not addressed the challenges of 3D indoor mapping in environments where GNSS signals are inaccessible. Furthermore, Tondaś et al. [12] and Hu et al. [13] developed data fusion methodologies with Kalman Filters, but their focus was more on data processing for land deformation monitoring and autonomous vehicle applications in outdoor conditions [12, 13]. These studies also did not discuss the use of integration between GNSS, IMU, and LiDAR for 3D indoor mapping that requires Ground Control Points (GCPs) for LiDAR data georeferencing.

This research aims to develop and analyze the integration of GNSS, IMU, and LiDAR using the UKF method for 3D indoor mapping purposes. This system is designed to overcome the limitations of the 3D models generated by Backpack LiDAR, which often lack position information because they cannot receive GNSS signals indoors. Without GCPs for georeferencing the three-dimensional data, the 3D model will only produce a local coordinate system that cannot be linked to a global reference frame, limiting its use for large-scale applications. Therefore, the GNSS, IMU, and LiDAR integration system will use IMU as a GCP in indoor environments to generate a more accurate 3D model that can be linked to the global reference frame. This research proposes an affordable solution that combines GNSS, IMU, and LiDAR technology, which has traditionally relied on expensive commercial equipment. By utilizing cheaper technology and precise sensor integration, it is hoped that 3D mapping for indoor environments can be performed effectively without relying on expensive equipment.

The main objective of this research is to develop and analyze the integration of GNSS, IMU, and LiDAR using the UKF method for 3D mapping in indoor environments. By combining data from various sensors, this system is expected to replace GNSS signals in indoor areas that are unreachable and provide the necessary GCPs for more accurate 3D mapping. With this technology, it is hoped that it will meet the broader indoor mapping needs without relying on expensive commercial systems.

The structure of this article is organized as follows. The first section, Methodology, will describe the approach and techniques used in this research, as well as the steps taken to achieve the research objectives. Next, the Materials and Methods section will explain the equipment used, data collection processes, and the analysis methods applied in this study. The GNSS-IMU Sensor Integration Algorithm section will discuss the algorithms and computational techniques used to integrate GNSS and IMU data for accurate geospatial positioning. Finally, the Results section will present the findings of this study, including data analysis, visualizations, and the interpretation of the results obtained.

2. Research Methodology

This research was conducted through several stages, beginning with data collection and followed by data fusion and analysis of the results. Data collection took place in an indoor environment using a Backpack LiDAR device, which was equipped with GNSS and IMU technology, as well as a Vision (Real-Time Kinematic) RTK2 device. The LiDAR sensor provided data in the form of point clouds that represent the geometry of the space, while the GNSS and IMU recorded information on position and orientation. The next stage involved data processing, where the raw data collected from the three sensors was processed. Notably, data from the IMU tends to drift or deviate from its actual position over time, so appropriate correction methods are necessary. Once the data has been processed, it will undergo a data fusion process utilizing the UKF [14]. The UKF method was selected due to its ability to manage non-linear uncertainties from sensor data. At this stage, data from GNSS and IMU will be combined to provide more accurate position estimates, even in conditions where GNSS may be unreliable. The final stage is Result Analysis, where the outcomes of data fusion will be evaluated to determine the system's accuracy [15]. The position and orientation results obtained will be compared to reference data or ground truth to assess the accuracy and reliability of the developed integration system.

Figure 1 shows the flowchart of the research methodology through which the objectives of this study were achieved.

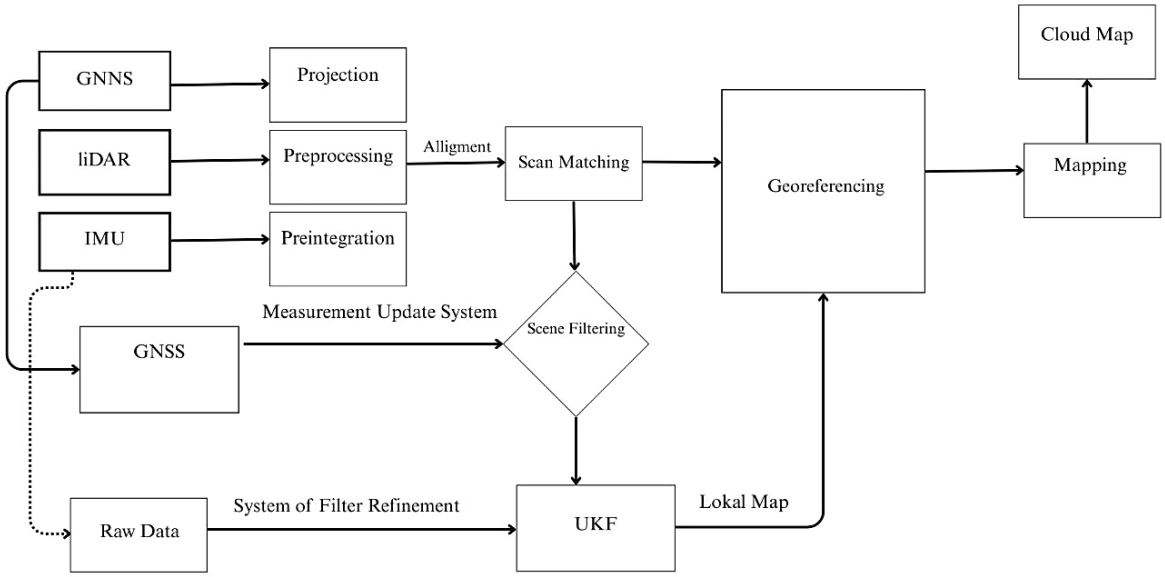

Figure 1. Technical framework of the system

The methodology used in this study aims to improve positioning accuracy in GNSS signal outage conditions by utilizing the IMU sensor. GNSS data is projected into UTM coordinates, IMU data undergoes unit conversion to the required format, and LiDAR data is processed through preprocessing steps. Afterward, the data from all three sensors is aligned through alignment and scan matching processes, aiming to match the visual features in the LiDAR data and improve position data congruence. The next step involves the Measurement Update System, where position information from GNSS is integrated with IMU data using scene filtering methods. This aims to update position estimates more accurately based on the processed data. Then, the results from this system are processed in the filter refinement stage to optimize position estimates, followed by applying the UKF method to reduce error covariance and further improve position estimate accuracy. After position estimates are obtained, this data is used for georeferencing LiDAR data, which then produces more accurate 3D maps. The georeferenced data obtained is then used in mapping to generate the final map with a high level of precision. By combining GNSS-IMU sensor fusion and LiDAR data, and using the UKF technique, this system successfully overcomes challenges posed by GNSS signal outage and urban environments that block GNSS signals, while enhancing the accuracy of position estimates in various conditions. The scheme adopts a “prediction + update” filter structure overall, with the number of updates specifically designed.

Additionally, GNSS is chosen directly as the update quantity in open areas, ensuring simple and effective accuracy in open spaces. In unobstructed open areas, differential GNSS can provide high-precision position information up to centimeter level, which is fully maintained and utilized in this scheme [2]. In urban environments, where GNSS signals are often obstructed by tall buildings or other structures, IMU can function more broadly and effectively. IMU measures acceleration and rotation, helping to estimate position and orientation even when GNSS signals are lost [3, 7]. In this scenario, the IMU works independently to track motion, providing continuous position estimates. However, while IMU is highly useful, the position accuracy it generates tends to degrade over time due to cumulative errors. Therefore, to improve overall accuracy, high-precision GNSS position data is integrated with IMU data. By combining both in a sensor fusion system, the position predicted by IMU is corrected using GNSS data when signals are available. This ensures that the system remains accurate even when GNSS signals are interrupted, and the quality of UKF filter updates is maintained, particularly in areas with weak or intermittent GNSS signals. This integration allows for higher positioning accuracy and system stability under various conditions.

3. Material and Methods

The data used in this study were collected from Vision RTK and Backpack LiDAR measurements conducted during outage conditions at the ITS Research Center Building, located at coordinates 7°16'52.10" south latitude and 112°47'50.91" east longitude. This dataset includes information recorded by GPS and IMU sensors from both the Vision RTK and Backpack LiDAR devices. The components of the Backpack LiDAR sensors are situated at the top of the Backpack frame, as illustrated in Figure 2.

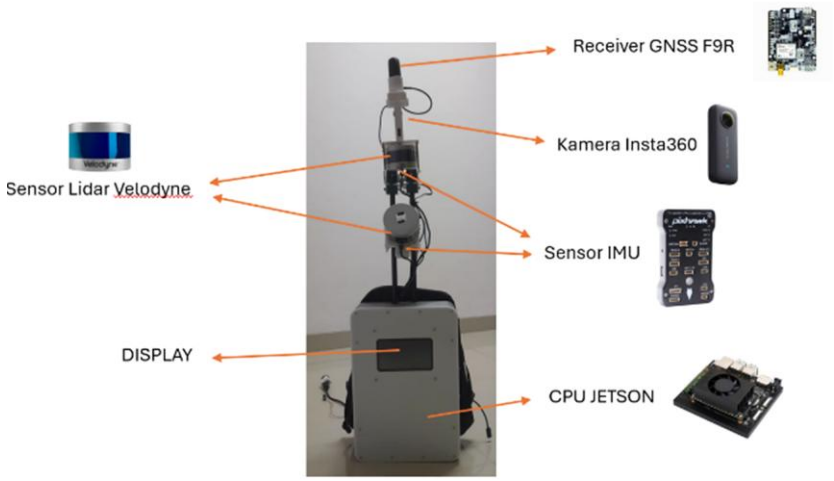

Figure 2. Backpack LiDAR uses GPS and IMU sensors as a navigation system

Vision-RTK2 is a development of RTK that combines computer vision, RTK-GNSS, inertial sensors (IMU), and odometer data as seen in Figure 3. The horizontal and elevation positioning accuracy of Vision-RTK2 is 1.0 cm + 1 ppm under fixed positioning conditions.

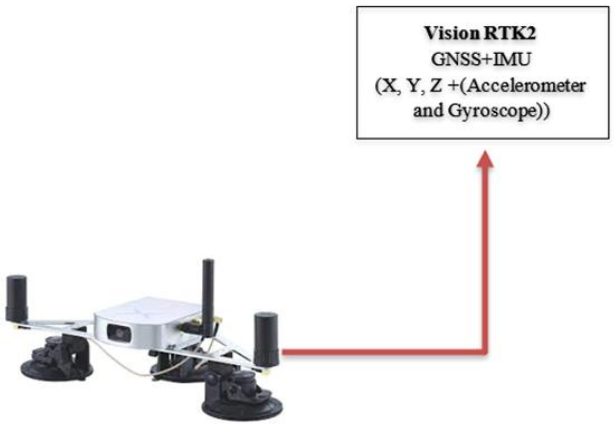

Figure 3. Vision RTK2 uses GPS and IMU sensors as a navigation system (Vision RTK, 2023)

4. GNSS-IMU Sensor Integration Algorithm

GNSS/IMU integration produces reliable position and navigation data. Sensor fusion increases productivity related to data availability during GNSS signal disruptions. In this study, sensor integration involves the use of 3 main parameters or 3 DOF. The 3-DOF car movement model for data collection was carried out at the Research Centre building of Institute Sepuluh Nopember, Surabaya for mapping purposes in indoor positioning with an average pedestrian speed of < 4.3 km/h. These attributes determine the location and direction of each observed epoch (Figure 4).

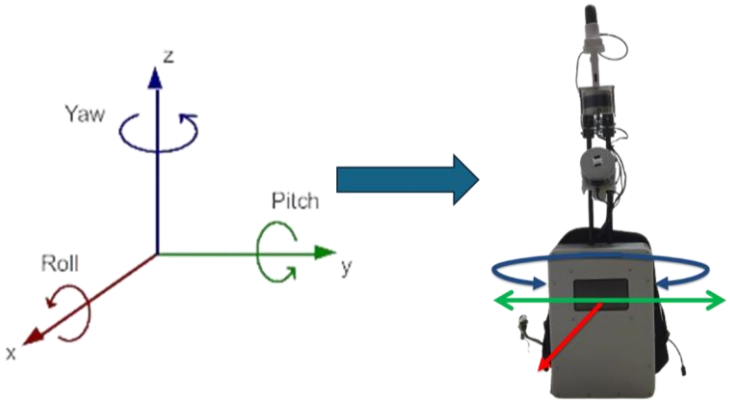

Figure 4. Three Degrees of Freedom of Motion for research

The following are the kinematic Equations used.

$$\dot{E} = u\sin(\psi) + v\,cos\,(\psi) \quad (1)$$

$$\dot{N} = u\cos(\psi) - v\sin\,(\psi) \quad (2)$$

$$\dot{\psi} = r \quad (3)$$

In those equations 'E' is for the position thelocal-level coordinate position at local-level coordinate on east direction and 'N' north is for north$u$' is the linear velocity on the 'E' and 'v' is thedirection. N' axes.'u/ yaw (rad) is symbolize by 'ψ is the the rotation on z-axes speed at n-frame (rad/s) is 'r'linear velocity on the dot notation $(\dot{})E$shows the derivative with respect to time' axes and 'v' is the linear velocity on the 'N' axes. The heading/ yaw (rad) is symbolize by 'ψ' and the rotation on z-axes speed at n-frame (rad/s) is 'r'. The dot notation $(\dot{})$ shows the derivative with respect to time.

The RTK position is determined in the northeast direction based on measurements from the accelerometer, which have been rotated into an n-frame. During epochs when GNSS data is available, the position estimated from the accelerometer measurements will be adjusted using the position obtained from GNSS observations. The yaw angle is determined from the rotational speed measured by the gyroscope. Data from the GPS and IMU sensors will be transmitted based on the movement of 3 DOF, which follows a kinematic model. The kinematic technique represents the movement of an object without considering the underlying reasons for that movement.

5. Result

This study utilized two primary methods for data acquisition: Vision RTK and Backpack LiDAR. Additionally, terrestrial measurements were conducted to determine the coordinates of the Ground Control Points (GCPs). The terrestrial measurements, carried out using a Total Station, are crucial for this study as they provide accurate reference points in the field. These GCPs are essential for validating the data obtained from Vision RTK and Backpack LiDAR, ensuring that the information is both accurate and reliable. A total of 8 GCP points were used, distributed throughout the research area (Figure 5). The coordinate data collection involved using a Total Station to establish tie points, which served as reference coordinates known beforehand. The control point coordinate data used to obtain position information can be found in Table 1.

Table 1. Easting and Northing coordinates from KKH calculations

Point	Easting (m)	Northing (m)
GCP-1	698471.187	9194804.499
GCP-2	698477.892	9194772.488
GCP-3	698462.720	9194725.672
GCP-4	698443.154	9194738.583
GCP-5	698418.770	9194727.195
GCP-6	698423.835	9194757.132
GCP-7	698415.504	9194771.372
GCP-8	698439.401	9194770.273

Sensor fusion processing using the UKF method is conducted with MATLAB software. The data processing in this study is divided into two parts: GNSS and IMU data processing. For GNSS data processing, e-frame coordinates are transformed into n-frame coordinates. In the case of the IMU, gyroscope measurements are integrated to obtain Euler angles. Additionally, coordinate transformation is applied to accelerometer measurements, followed by double numerical integration of the accelerometer data.

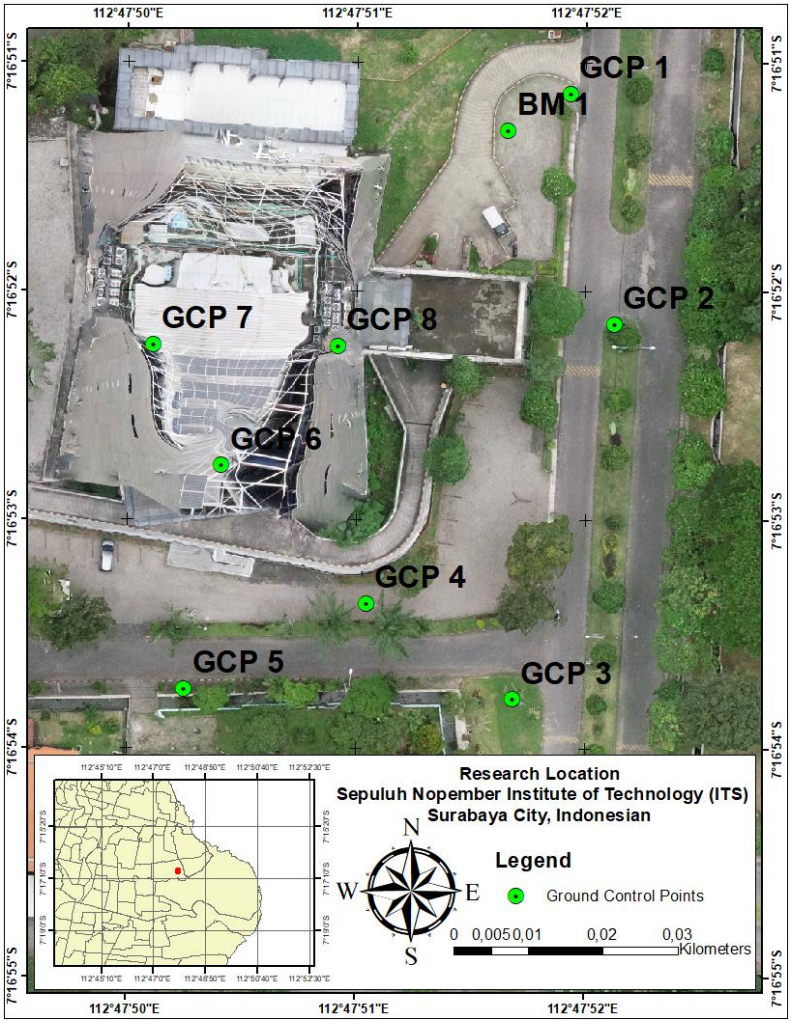

Figure 5. Distribution of Ground Control Points (author's property)

The mathematical model of the movement shown in Equations 1 to 3 is a continuous time system model. In order to define the system model and measurement model in the UKF simulation, the mathematical model needs to be discretized. Discretization is carried out using the Forward Finite Difference method because the UKF simulation to be carried out in this study aims to estimate the future time k. The Forward Finite Difference equation is written as follows:

$$\frac{da}{dt} = \frac{a_{k+1} - a_i}{\Delta t} \tag{4}$$

$$a_{k+1} = \frac{da}{dt}\Delta t + a_k \tag{5}$$

where xk+1 is the estimate of the state variable (X) at time k+1 observed at k. $\frac{da}{dt}$ is shows the rate of change of the first derivative of variable 'a' with respect to time 't'. The results of the mathematical model discretization that states the easting, northing, and yaw coordinate positions are:

$$\begin{bmatrix} E_{k+1} \\ N_{k+1} \\ \psi_{k+1} \end{bmatrix} = \begin{bmatrix} \Delta t\ (\mathrm{u}_k \sin(\psi) + v_k \cos(\psi) + E_k \\ \Delta t\ (u_k \cos(\psi) - v_k \sin(\psi)) + N_k \\ \Delta t\ r_k + \psi_k \end{bmatrix} \tag{6}$$

The results of the discretization indicate that a single-variable equation depends on multiple variables, which is characteristic of nonlinear equations. The model initially overlooks the presence of noise or disturbances. Although the noise is minimal, it is essential to consider its effects. By incorporating the noise term w_k into Equation 6, we can express the equation in a state space format that aligns with the system model of the UKF method, as shown in the following Equation.

$$X_{k+1} = f(x) + w_k \tag{7}$$

So, the UKF system model can be written as:

$$[x_{k+1}] = \begin{bmatrix} f_1 \\ f_2 \\ f_3 \end{bmatrix} + w_k \tag{8}$$

$$[x_{k+1}] = \begin{bmatrix} E_{k+1} \\ N_{k+1} \\ \psi_{k+1} \end{bmatrix} + w_k \tag{9}$$

$$\begin{bmatrix} E_{k+1} \\ N_{k+1} \\ \psi_{k+1} \end{bmatrix} = \begin{bmatrix} \Delta t\ (\mathrm{u}_k \sin(\psi) + v_k \cos(\psi) + E_k \\ \Delta t\ (u_k \cos(\psi) - v_k \sin(\psi)) + N_k \\ \Delta t\ r_k + \psi_k \end{bmatrix} + w_k \tag{10}$$

In the equations above, X_{k+1} is the unknown parameter that being estimated in this research. The E_{k+1} is the unknown parameter for east axes. UKF, while more accurate for nonlinear systems than EKF, is still sensitive to initial condition settings and covariance matrix tuning. Improper configurations can degrade performance, especially under degraded signal conditions. The effectiveness of UKF heavily depends on data quality and initial conditions [16]. In scenarios where GNSS corrections are unavailable, particularly during signal outages, the UKF algorithm must rely solely on the IMU data. This reliance can lead to increased errors, as the IMU's drift accumulates without the benefit of GNSS corrections, resulting in higher RMSE and MAE values observed during outages.

Moreover, UKF is particularly effective in handling nonlinearities inherent in sensor data. However, its performance remains contingent on the accuracy of the data it receives. During outages, when the UKF is forced to rely on less accurate IMU data, the results can be significantly compromised. This dependency on IMU data during outages often contributes to the elevated RMSE and MAE values observed in the system's performance [17].

5.1. Positioning During Outage Conditions

This study conducted a simulation using the UKF method under two conditions: free outage and outage conditions, by crossing the same location. During the outage conditions, data from IMU processing was utilized to obtain east and north positions. The results from this analysis will be compared with field data. In this study, IMU data was used to estimate positions during the outage period. The IMU provides acceleration and angular velocity data, which can be integrated to estimate changes in position and orientation. However, due to the inherent drift of the IMU, errors in position estimation will increase over time if no external data corrections are applied.

The large RMSE and MAE values observed during outage conditions can be attributed to several factors, primarily stemming from sensor limitations. First, IMU drift becomes a significant issue when GNSS corrections are unavailable. The IMU, relying solely on its internal accelerometer and gyroscope sensors, tends to accumulate errors over time, with small initial inaccuracies becoming magnified, resulting in increasingly larger positioning errors. This drift is particularly evident during outage conditions, where the IMU operates without the benefit of GNSS corrections, leading to substantial errors as reflected in the high RMSE and MAE values [16, 18]. Moreover, in indoor environments or areas where GNSS signals are blocked or weakened, the IMU operates in isolation, further exacerbating the accuracy loss. The absence of GNSS signals forces the IMU to operate independently, but without external corrections, the positioning accuracy degrades significantly over time [19, 20].

To address these limitations, The UKF method is used to combine data from the IMU with the last data received from the GPS before the outage occurred. The UKF has better performance in non-linear estimation problems due to its use of the unscented transform, this also improve the estimation accuracy [20]. The UKF method was more accurate in captures the mean and covariance of a probability distribution than linearization techniques in the EKF. UKF does not require the derivation of Jacobian matrices, that was why it more robust and easier to implement in complex systems such as GNSS-IMU integration [3]. The UKF method that can handle nonlinearities without linearization contributed to this significant improvement. During the outage period, position predictions are obtained by integrating IMU data and using UKF to update position estimates based on a 3 DOF kinematic model. The following are the trajectory results from IMU data processing using the Euler method in the Research Center Building Area in Simulation II presented in Figure 6.

In Figure 7, the accuracy of the IMU data processing during outage conditions remains poor. To quantitatively assess the level of accuracy, we calculate the Root Mean Square Error (RMSE) and Mean Absolute Error (MAE). The RMSE value is derived from the average of the estimation results compared to the measurement data, allowing us to evaluate the accuracy of the estimates.

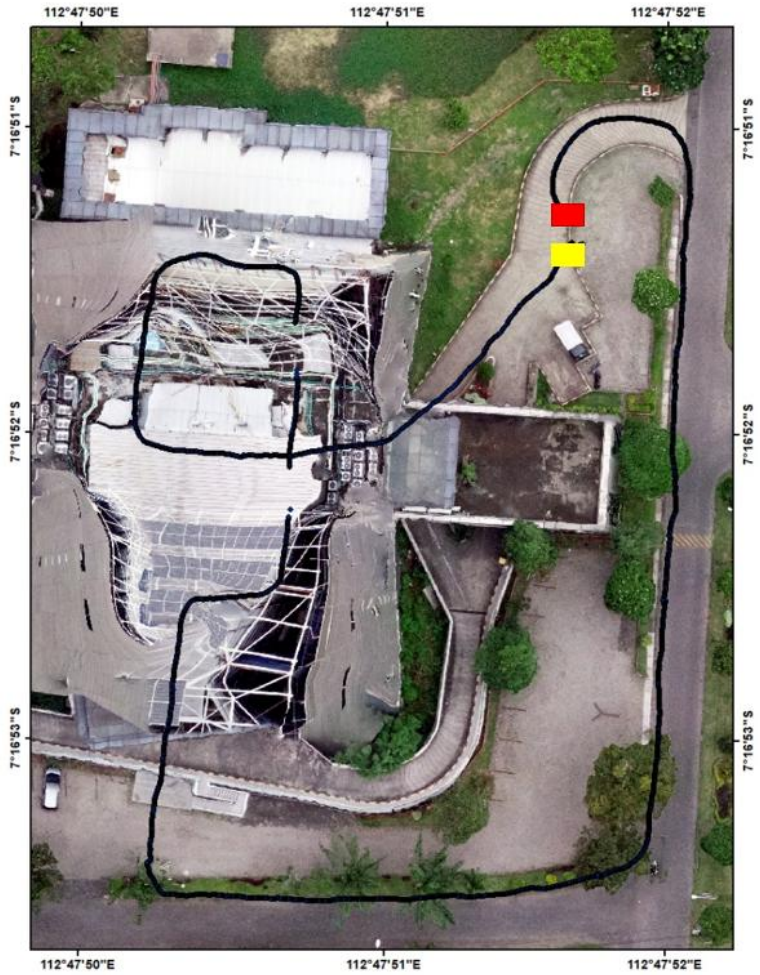

Figure 6. Trajectory of data collection path by walking, the red city is the start, and the yellow city is the stop

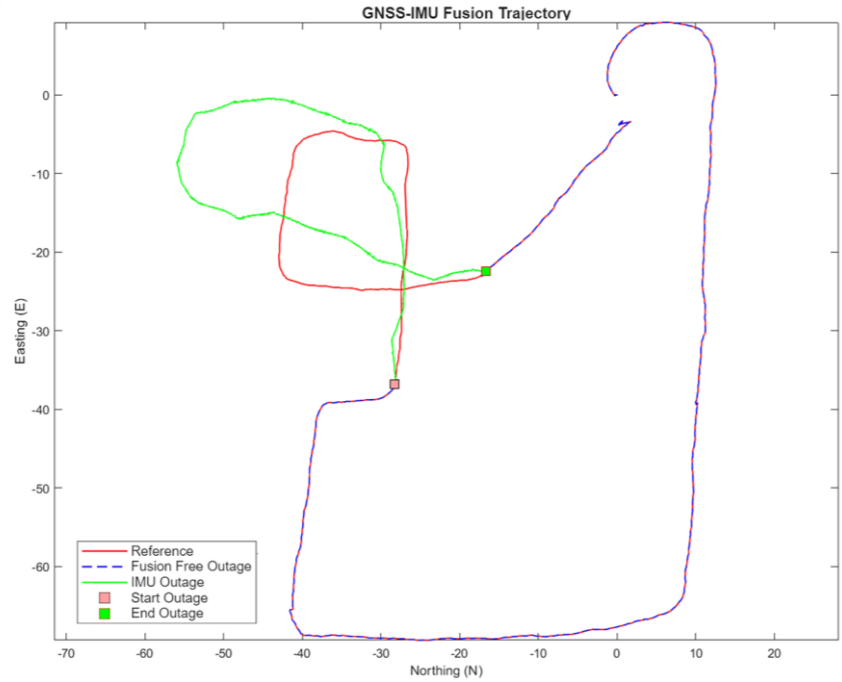

Figure 7. Trajectory of the Research Center Building during GNSS Signal Outage (author's property)

In this study, we employed Root Mean Square Error (RMSE) and Mean Absolute Error (MAE) as evaluation metrics to assess the accuracy of the GNSS-IMU data fusion system utilizing the UKF method, as previously demonstrated in

similar research. These metrics were specifically selected due to their ability to quantify the discrepancy between estimated and reference (ground truth) positions, a method widely used in geospatial studies [16, 19].

RMSE is particularly sensitive to large errors, as it gives greater weight to outliers. A higher RMSE value typically indicates substantial deviations between the estimated and true positions, which can be attributed to significant errors during data collection, sensor limitations, or environmental interference, as noted by Yang et al. [16]. Conversely, MAE measures the average magnitude of errors without considering their direction, offering a simpler representation of the overall error across all data points.

In Free Outage Conditions, where GNSS signals are uninterrupted, the results showed low RMSE values of 0.00308 m for Easting and 0.00175 m for Northing, along with MAE values of 0.00088 m for Easting and 0.00024 m for Northing. These values indicate very high accuracy in positioning estimates, consistent with expectations given the availability of both GNSS and IMU data for fusion without external interference [17, 20].

The RMSE and MAE values during the outage conditions, as presented in Table 2, indicate that positioning using the IMU has not resulted in position estimates with errors exceeding 1 meter. The trajectory generated by the IMU closely resembles the reference trajectory and follows the same pattern. However, as shown in Table 4.7, the RMSE and MAE values are significantly large, measuring 4.0881 meters and 8.6317 meters at the easting, and 5.9871 meters and 7.4182 meters for the northing.

Table 2. RMSE and MAE values under GNSS Signal Outage conditions

Positioning	RMSE (m)		MAE (m)	
	Easting (E)	Northing (N)	Easting (E)	Northing (N)
IMU Processing during Outage	4.0881	8.6317	5.9871	7.4182

In this context, several factors contribute to the increased RMSE and MAE values during signal outages. First, the IMU sensor is subject to drift over time, which becomes more pronounced when external corrections from GNSS are unavailable. This drift accumulates, leading to larger positional errors during the outage period. Additionally, the environmental factors such as physical obstructions, multipath effects, and GNSS signal interference also exacerbate these errors. Research by Cahyadi et al. [3] found that the fusion of GNSS and IMU data during outage conditions resulted in a relatively large error of 34.49 meters. According to Cahyadi et al. [4], loosely coupled integration has limitations in providing accurate position estimates because, when stand-alone GNSS does not provide any position information, no external data is available to correct the IMU measurements. As a result, the IMU error accumulates even further, leading to larger errors, as seen in this study.

The performance of the UKF method, while generally superior to the EKF in handling non-linearities and sensor noise, is still influenced by the initial configuration and the choice of parameters. For example, the process and observation noise covariance matrices, which are crucial to the UKF's performance, can affect the accuracy of the fused results. In the absence of real-time GNSS updates during outage conditions, relying solely on IMU data leads to accumulating errors, as evidenced by the significantly large RMSE and MAE values. While the UKF method shows better performance, its effectiveness depends on the quality of input data and the configuration of noise parameters. At this stage of the research, the proposed approach is still offline or post-processing, where data processing is carried out after all data is collected in the field. This is being done to validate the effectiveness of the UKF method in improving the accuracy of position estimation, especially in complex indoor environments [21]. Theoretically, the UKF algorithm has a level of computational complexity that still allows it to be implemented in real-time systems [22], such as autonomous drones or robotic navigation.

5.2. Positioning During Free Outage Conditions

Environmental conditions, such as indoor settings with obstacles or reflective surfaces, can significantly impact the reception of GNSS signals. Multipath effects, where GNSS signals reflect off surfaces and cause erroneous readings, can degrade the accuracy of GNSS measurements. In situations with poor satellite visibility (e.g., indoor environments with obstructed lines of sight), GNSS measurements may become highly unreliable, further increasing the error in the system [17, 23]. Similarly, physical obstructions in densely built areas, GNSS signals can also be blocked by walls or other large structures, making it difficult for the system to maintain accurate position estimates. This explains the increase in RMSE and MAE during the signal outage conditions [23].

In free outage conditions, GNSS signals are continuously available without interruption. Sensor fusion combines data from GNSS and IMU to enhance the accuracy of position and orientation estimates. The UKF updates these estimates in real-time, using GPS data as a correction to minimize the cumulative errors of the IMU. At each time step, position data from GPS is utilized to refine the position predictions derived from the integration of IMU data, thereby reducing drift and other errors that may arise in the IMU.

The validation results indicate that the UKF method effectively integrates data from GNSS and IMU, yielding robust and accurate estimates of position and orientation even in conditions where GNSS signals are unavailable. As shown in Figure 8, the trajectory generated by the Vision RTK2 tool is quite impressive, successfully estimating the position during GNSS signal outages in a parking lot obstructed by tall buildings. The UKF estimation, utilizing GNSS and IMU data from Vision RTK2, combined with 3 DOF modelling, produces a highly accurate trajectory that closely aligns with the measurement data. In the UKF calculations, a comparison is made between each measurement variable and the results of the UKF estimations (Figure 9). This comparison is illustrated in the following graph.

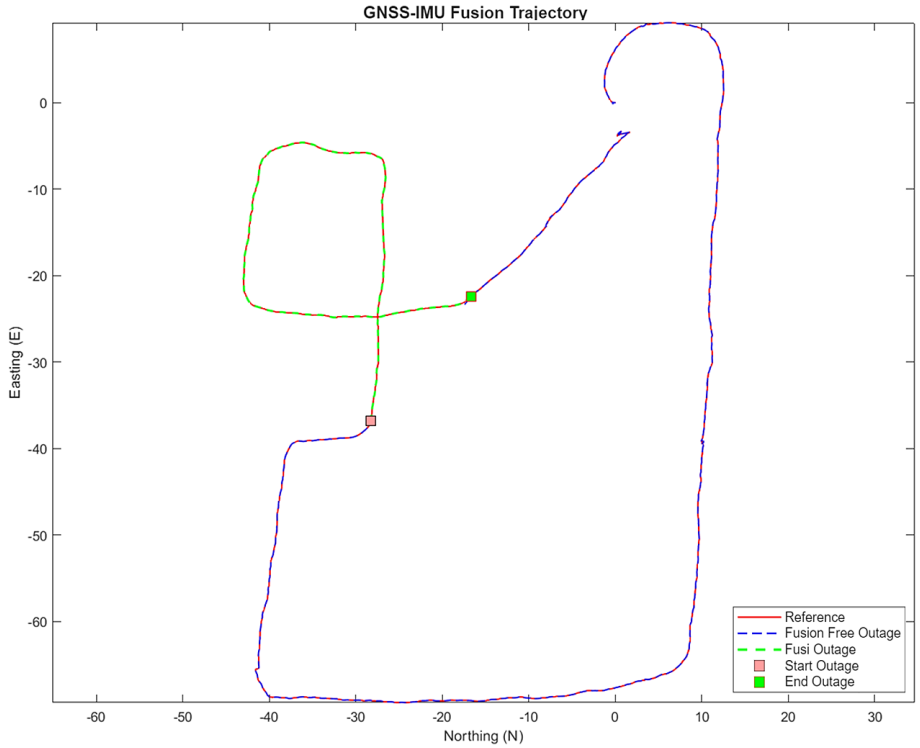

Figure 8. Trajectory of the Research Center Building when Free Outage Conditions

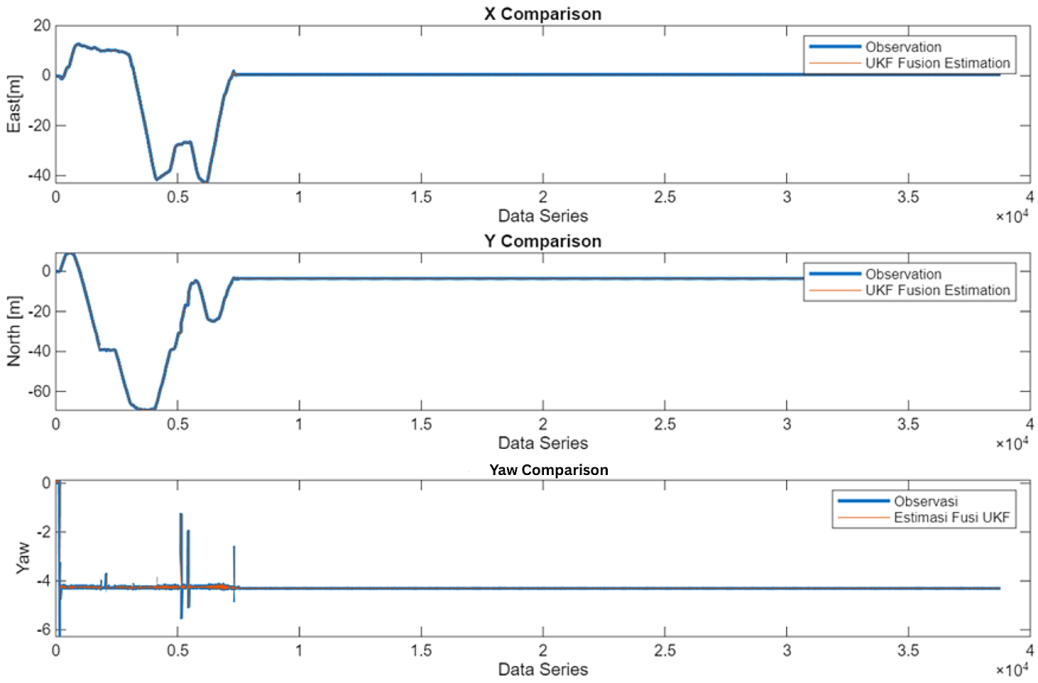

Figure 9. Comparison Graph of Observation Variables and UKF Estimation

Based on the UKF simulation results displayed in the graph, the position estimates obtained are close to the measurement data with relatively small deviations. This shows that the UKF method is able to provide accurate results under certain conditions. To provide a clearer picture of the system performance, Table 2 presents the RMSE and MAE values under Free Outage conditions.

Table 3 presents the RMSE and MAE values as 0.00308 m and 0.00088 in easting, which are close to the values of 0.00175 and 0.00024 in northing. According to the RMSE and MAE Interpretation Guidelines mentioned earlier, these values fall within the error level of 0.000 m - 0.299 m, indicating a small error. The MAE and RMSE values generated by the UKF method are very low, nearly approaching zero. This highlights that the estimation results from the UKF are qualitatively very good and accurate. Furthermore, the MAE value aligns with the RMSE results: in the easting measurement, the value is greater than that in northing, which is also observed in the corresponding MAE values.

Table 3. RMSE and MAE values under GNSS conditions when the condition is Free Outage

Variable	RMSE (m)	MAE (m)
Easting (E)	0.00308	0.00088
Northing (N)	0.00175	0.00024

Following Table 3, the performance of the GNSS-IMU data fusion system under Free Outage Conditions demonstrated high accuracy, with very low RMSE and MAE values for both Easting and Northing. These results indicate a close alignment between the estimated positions and the reference positions, as expected when both GNSS and IMU data are available for fusion without external interference However, when GNSS signals were unavailable during Signal Outage Conditions, a noticeable increase in the RMSE and MAE values was observed. Specifically, RMSE values rose to 4.0881 m for Easting and 8.6317 m for Northing, while MAE values reached 5.9871 m and 7.4182 m, respectively. This significant increase underscores the challenges of relying solely on IMU data during outages. Without GNSS corrections, the IMU data, which tends to drift over time, resulted in substantially larger positional errors [20].

While this study demonstrates improved accuracy, the practical implementation of the GNSS and IMU data fusion system for real-time vehicle navigation systems faces several challenges. One of the key issues is the requirement for fast data processing, which can be a limitation when using hardware with limited computational capacity. Additionally, the performance of the UKF method is highly dependent on the quality of the sensor data and the initial system configuration. Environmental factors, such as GNSS signal interference or poor satellite visibility, can also affect the accuracy of the system. However, with advancements in processing speeds and better management of signal disruptions, this data fusion approach shows potential for application in vehicle navigation systems, especially in areas with limited GNSS signal availability, such as urban canyons or areas with dense buildings [24, 25].

5.3. 3D Visualization of Backpack LiDAR Model

3D visualization of the model generated from Backpack LiDAR data provides a detailed picture of the topography and surface features of the mapped area. The 3D visualization process of Backpack LiDAR data includes the georeferencing process of point cloud results with trajectories resulting from previous UKF processing and KKH calculations. From the IMU sensor, data is obtained in the form of accelerometers, gyros, and magnetometers where the program has carried out data integration between data obtained from LiDAR (distance data and angle to the sensor) with IMU data, time is used as a link which is called SLAM (Simultaneous Localization and Mapping). The data acquisition process involves first observing the area to be surveyed. If the area is dynamic, the data collection will be divided into several segments, which will later be merged. The LIOSAM algorithm assists the system in handling long-duration data collection by performing corrections based on previous and current data timestamps [26, 27].

The 3D model processing is preceded by the LiDAR data georeferencing process with data obtained from Total Station measurements. Point cloud georeferencing is carried out to produce accurate spatial data, as well as to register data to have the desired UTM reference. The georeferencing process is carried out at the point in the KKH calculation which is used as the GCP as a control point (see Figure 10). After georeferencing, the RMSE value is obtained as in Table 9.

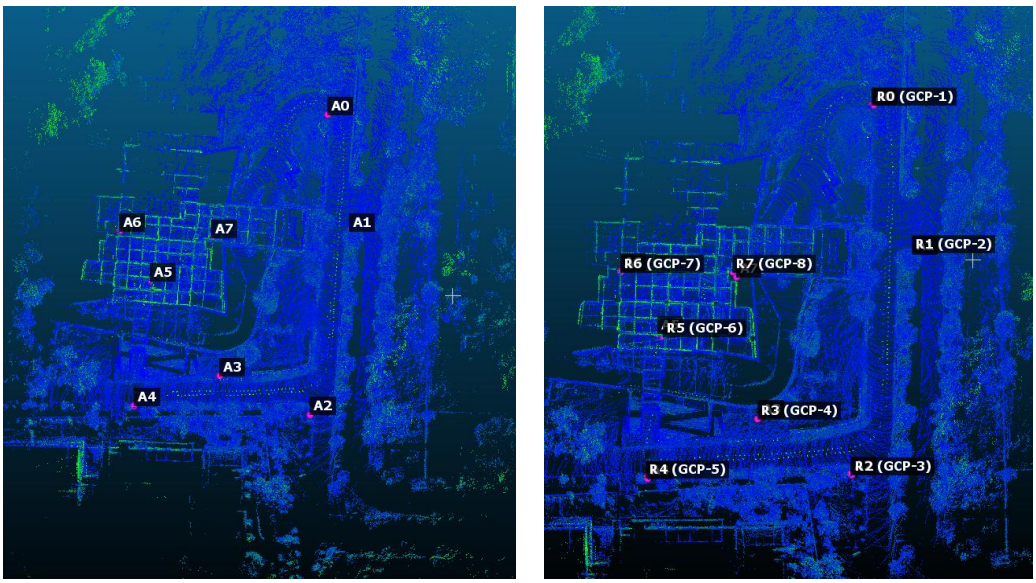

(a) (b)

Figure 10. Georeferencing: a) placement of points on the point cloud and b) GCP points as references

After obtaining the error value of each point, the RMSE calculation is carried out, namely taking the square root of the average square error of all GCPs. To provide a clearer picture of the error value, Table 4 presents the RMSE value after georeferencing.

Table 4. Georeferenced RMSE Values

Variable	RMSE (m)
Georeferencing LiDAR Data with Total Station Measurement Data	0.3420
Georeferencing LiDAR Data with UKF Sensor Fusion Measurement Data	0.6358

During the LiDAR data processing for georeferencing, several limitations were encountered, including signal interference and data noise due to moving objects, as well as the lack of GCP in indoor environments where GNSS signals were unavailable. These challenges were addressed by performing noise-cleaning on the point cloud data to remove irrelevant objects, and by integrating GNSS and IMU data using the UKF for sensor fusion, which allowed for the estimation of positions and provided the necessary GCPs. Additionally, the georeferencing process was enhanced by combining KKH calculations and UKF fusion data, yielding accurate results with RMSE values of 0.3420 m for KKH and 0.6358 m for UKF fusion, demonstrating high alignment with reference measurements. These steps ensured the accuracy and reliability of the georeferenced LiDAR data, effectively addressing the observed limitations.

Further enhancing this approach, the integration of LiDAR, IMU, and GNSS sensors using the LIO-SAM method has shown promise for indoor mapping in GNSS-denied environments. In the study conducted by Triawan et al. [28], the accuracy achieved using the LIO-SAM method with the integration of LiDAR, GNSS, and IMU sensors showed excellent results. Based on the comparison of tree diameter and height measurements between direct and LiDAR-based methods, the study reports a RMSE (Root Mean Square Error) of 0.0003 meters for horizontal measurements and 0.0004 meters for vertical measurements. Furthermore, the standard deviation (STDV) for horizontal measurements was 0.014 meters, while for vertical measurements, it was 0.011 meters. These results demonstrate very high accuracy, with errors on the millimeter scale, making the system highly reliable for applications that require high precision, such as tree inventory and forest mapping. While this method improves mapping performance over traditional TLS and ALS methods, the addition of camera-based SLAM or barometers can further improve robustness in challenging environments.

The accuracy of LiDAR data is tested according to the ASPRS Positional Accuracy Standards for Digital Geospatial Data, Edition 1, November 2014, as well as PERKA BIG No. 6 of 2018, which amends the Regulation of the Head of the Geospatial Information Agency Number 15 of 2014 concerning Technical Guidelines for Base Map Accuracy. The analysis of accuracy testing includes both absolute accuracy and relative accuracy. The LE value is determined after calculating the RMSE value. Once the RMSE value has been obtained, you can proceed to calculate the LE value using the following formula.

$$CE_{90} = 1.5175 \times RMSE \tag{11}$$

Based on the georeferencing results obtained, namely RMSE of 0.3420 meters for KKH and 0.6358 meters for UKF results, we can calculate the vertical accuracy (LE90) using the BIG standard conversion factor.

$$CE_{90KKH} = 1.5175 \times 0.3420 = 0.5189 \quad (12)$$

$$CE_{90UKF} = 1.5175 \times 0.6358 = 0.9648 \quad (13)$$

Based on Equation 12 and 13, the RMSE value of 0.3420 meters with a value of $LE_{90} = 0.5189$ is suitable for map scales between 1:1,000 and 1:2,500. This number shows that the georeferencing results on KKH meet the criteria for high accuracy and are suitable for map scales with very good detail. However, the RMSE value of 0.6358 with a value of $LE_{90} = 0.9648$ is suitable for map scales between 1:2,500 and 1:5,000. This number indicates that the georeferencing results on UKF are in the moderate accuracy category and are suitable for larger map scales with lower detail compared to KKH.

For the RMSE on the KKH, which is 0.3420 meters, the conversion of this value into horizontal accuracy in centimeters is 34.20 cm, which means that this accuracy is between the map scale of 1:1,200 to 1:1,800, indicating that the georeferencing on the KKH has higher accuracy and is suitable for map scales with very good detail. This shows that the KKH georeferencing results meet or even exceed the accuracy tolerance required for larger map scales, ensuring that the resulting map data is very accurate for applications that require high detail. Meanwhile, for the RMSE on the UKF results, which is 0.6358 meters or 63.58 cm, this accuracy is suitable for map scales between 1:2,000 to 1:3,000 according to the ASPRS standard. This means that the georeferencing performed on the UKF is in the medium accuracy category and is suitable for larger map scales, with less detail compared to the results on the KKH. Although the georeferencing on the UKF results is still within the acceptable tolerance range, the results show lower accuracy compared to the KKH, making it more suitable for applications that do not require the level of detail as high as that obtained from the KKH.

Based on Table 5, the overall georeferencing accuracy, following ASPRS standards and BIG regulations, falls within class 2 map geometry accuracy. This indicates that at least 90% of the positional errors or shifts in objects on the 1:1,000 Scale RBI Map do not exceed one meter in the horizontal position. Furthermore, the results from the KKH demonstrate a higher level of detail, meeting the accuracy requirements for a smaller map scale, while the UKF results are within a moderate tolerance range, making them suitable for a map scale with lower detail. This analysis ensures that the map produced from the georeferencing process satisfies the accuracy needs for its intended application and adheres to the established standards for map accuracy.

Table 5. Map Scale Classification Results

Data Types	Map Scale and Class (BIG)	Map Scale (ASPRS 2014)
LiDAR with Total Station Data	1:1,000 Class 2	1:1,200
LiDAR with UKF Fusion Data	1:2,500 Class 2	1:2,000

5.4. Comparison of Distance with LiDAR and Ground Truth

The measurement data obtained from a meter is regarded as the ground truth. This meter data is compared with LiDAR data prior to georeferencing. The LiDAR data is georeferenced using KKH calculation data and also through UKF fusion data. This process allows us to calculate the Root Mean Square Error (RMSE), which indicates the amount of error present in the LiDAR data. The details of the calculations can be found in Table 5:

Column a is the LiDAR data before georeferencing, column b is the LiDAR data georeferenced with the GCP points calculated by KKH, and column c is the LiDAR data that has been georeferenced with the UKF fusion results. From the results of the distance comparison in Table 6, it is known that the distance dimensions are respectively 0.5701 m, 0.0354 m, and 0.0779.

Table 6. Comparison table of Point Cloud Distance dimensions

No	Distance	Roll Meter (m)	Point Cloud			Difference With Roll Meter			$(Difference)^2$		
			a	b	c	a	b	c	a	b	c
1	Distance 1	5.97	5.85	5.99	5.88	0.12	-0.02	0.09	0.0144	0.0004	0.0081
2	Distance 2	9.24	9.59	9.14	9.07	-0.35	0.1	0.17	0.1225	0.01	0.0289
3	Distance 3	4.67	4.56	4.63	4.69	0.11	0.04	-0.02	0.0121	0.0016	0.0004
4	Distance 4	3.95	3.96	3.88	3.75	-0.01	0.07	0.2	0.0001	0.0049	0.04
5	Distance 5	2.2	1.89	2.16	2.19	0.31	0.04	0.01	0.0961	0.0016	0.0001
6	Distance 6	3.75	3.18	3.62	3.77	0.57	0.13	-0.02	0.3249	0.0169	0.0004
					RMSE				0.5701	0.0354	0.0779

The RMSE values indicate that the georeferenced LiDAR measurements, derived from the KKH and Roll Meter Calculations, have the smallest RMSE. This suggests a high level of agreement between the point cloud data and the measurements taken with the roll meter, which serves as the reference data. To analyze the relationship between the roll meter and the LiDAR data, a linear regression plot was created. If the line representing the LiDAR dimensions aligns closely with the line from the roll meter, it indicates a strong relationship between the two variables. Therefore, better regression fit corresponds to higher accuracy in the LiDAR data. Figure 11 presents the results of the linear regression plot for these two datasets.

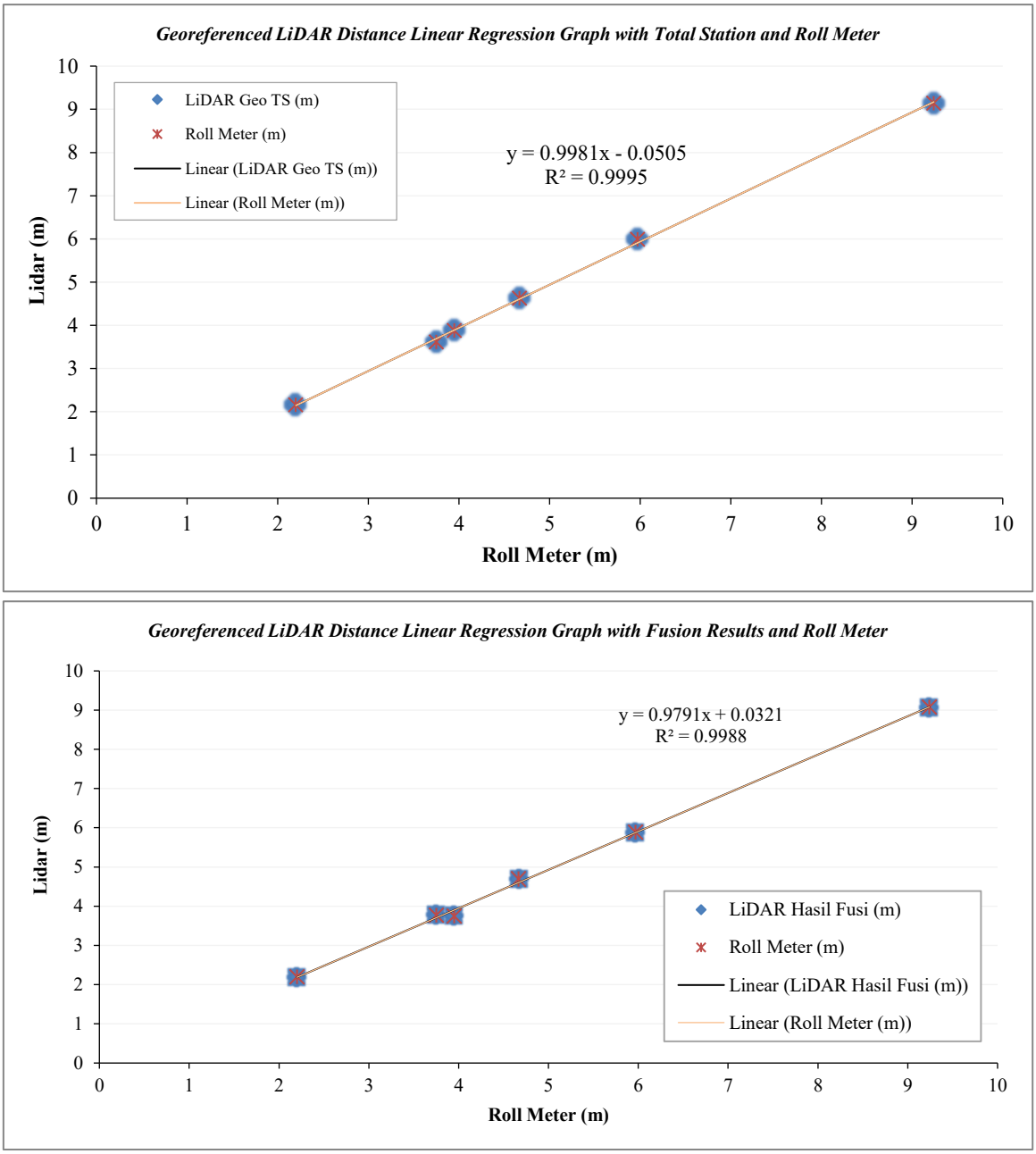

Figure 11. Linear regression graph of LiDAR distance

Based on Figure 11, both graphs show a very strong linear relationship between the distance measured by LiDAR and the roll meter. Although both methods (georeferencing with Total Station and data fusion results) produce a very strong linear relationship, the results from Total Station georeferencing are slightly closer to 1 in terms of slope compared to the data fusion results. The very high R^2 values in both graphs indicate that both methods are very reliable in measuring distance compared to the roll meter. The regression equation shows that the Total Station georeferencing method is slightly more accurate in approaching a 1:1 linear relationship with the Roll Meter.

The 3D LiDAR model is visualized after going through a noise-cleaning process on the point cloud data, which previously contained moving objects recorded by the sensor. This process ensures that the visualization results only reflect static and relevant objects in the survey area. The final visualization of the processed data, as shown in Figure 12.

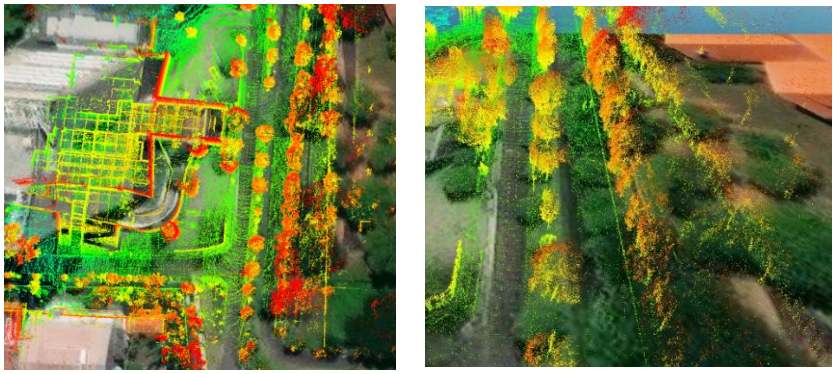

(a) (b)

Figure 12. 3D LiDAR model results: (a) Top View, (b) Road View

According to Figure 12, various objects such as trees, buildings, and roads can be observed. The visualization of the LiDAR data exhibits a recognizable level of detail, including the shape of roofs, stairs, and text, without reliance on thematic objects. The point cloud's density allows for the identification of building details, such as the location of doors, fences, and roof shapes. Therefore, it is clear that the object in question is a building.

In our study on indoor mapping using GNSS, IMU, and Backpack LiDAR, we integrated these sensors using the UKF method to improve 3D mapping accuracy in environments where GNSS signals are unavailable. Our results show that the UKF method, combined with LiDAR, outperforms traditional methods like EKF. Compared to previous studies, such as the one by Cahyadi et al. [29], hich conducted the fusion of GNSS and IMU sensors on vehicle navigation, the results of east and north position accuracy at Transmart Sidoarjo and Royal Plaza were 3.556 m and 6.709 m, as well as 6.364 m and 8.465 m, respectively. Compared to standalone GNSS, in free outage conditions, fusion using SPP/IMU increased the accuracy of east and north positions by 68.28% and 66.64%, respectively. Conversely, DGNSS/IMU fusion improved the accuracy of east and north positions to 93.02% and 93.03%, respectively. Additionally, previous studies, such as the one by Navisa et al. [18], which explored UKF integration for medical drones, show that UKF integration outperformed EKF, with an accuracy of 0.022 meters, far surpassing the 8.467 meters achieved by the EKF method in similar conditions. By incorporating LiDAR into our fusion system, we have achieved a new level of positioning accuracy, especially under signal outage conditions, which has not been fully addressed in the existing literature.

Based on the results and analysis conducted, it can be concluded that the integration of the UKF method with GNSS and IMU data fusion has successfully improved position estimation accuracy, especially in free outage conditions. The accuracy achieved in these conditions shows very low RMSE values, with 0.00308 m for Easting and 0.00175 m for Northing, as well as small MAE values. However, in signal outage conditions, the position estimation accuracy from IMU data significantly decreased, with RMSE reaching 4.0881 m for Easting and 8.6317 m for Northing, indicating that IMU data alone is less capable of providing accurate position information. Nevertheless, GNSS-IMU fusion with the UKF method in signal outage conditions still produces trajectories that are close to the reference, although the accuracy obtained is not optimal. Furthermore, the validation of the georeferenced 3D LiDAR model using UKF data fusion and KKH calculations showed satisfactory results, with small RMSE values of 0.3420 m and 0.6358 m, indicating a high level of agreement between point cloud data and reference measurements. Therefore, this study proves that the use of a combination of GNSS, IMU, and LiDAR through the UKF approach is a promising solution to improve 3D mapping accuracy in indoor environments, although challenges remain in non-optimal GNSS signal conditions.

6. Conclusion

In this study, we explored the integration of GNSS, IMU, and Backpack LiDAR using the UKF to improve indoor positioning accuracy, particularly in environments where GNSS signals are limited. The fusion of GNSS and IMU data through the UKF method significantly enhanced position estimates during free outage conditions, achieving low RMSE values of 0.00308 m for Easting and 0.00175 m for Northing, and small MAE values, indicating highly accurate position tracking. However, during signal outages, the performance of the system deteriorated, with RMSE values reaching 4.0881 m for Easting and 8.6317 m for Northing, as the IMU data alone became less reliable due to drift accumulation. Despite this, the UKF method still produced trajectories that were close to the reference data, confirming its potential for improving navigation accuracy even under challenging conditions. The integration of LiDAR provided valuable 3D point cloud data, which, when georeferenced using UKF fusion data and KKH calculations, showed strong alignment with reference measurements, as evidenced by RMSE values of 0.3420 m for KKH and 0.6358 m for UKF fusion results. This research highlights the effectiveness of combining GNSS, IMU, and LiDAR technologies to overcome the limitations of GNSS signals in indoor environments. While the proposed method significantly improved position estimation accuracy, further research is necessary to address the limitations posed by IMU drift during signal outages and to enhance the real-time applicability of the system. The findings contribute to the development of cost-effective and accurate indoor navigation systems, which can be applied in various settings such as industrial facilities, shopping malls, and other environments where GNSS signals are typically unavailable.

7. Declarations

7.1. Author Contributions

Conceptualization, Q.P.A.N.I. and M.N.C.; methodology, Q.P.A.N.I. and T.A.; software, H.F.S.; validation, M.N.C., T.A., and H.F.S.; formal analysis, Q.P.A.N.I.; investigation, Q.P.A.N.I.; resources, T.A. and H.F.S.; data curation, Q.P.A.N.I., M.N.C., T.A., and H.F.S.; writing—original draft preparation, Q.P.A.N.I.; writing—review and editing, M.N.C. and F.T.; visualization, Q.P.A.N.I.; supervision, M.N.C., T.A., and H.F.S.; project administration, M.N.C.; funding acquisition, M.N.C. All authors have read and agreed to the published version of the manuscript.

7.2. Data Availability Statement

The data presented in this study are available in the article.

7.3. Funding and Acknowledgements

The authors gratefully acknowledge financial support from the Institut Teknologi Sepuluh Nopember for this work, under the project scheme of the Publication Writing and IPR Incentive Program (PPHKI) 2024, contract number 64/IT2/T/HK.00.01/X/2024.

7.4. Conflicts of Interest

The authors declare no conflict of interest.

8. References

[1] Syazwani, C. J. N., Wahab, N. H. A., Sunar, N., Ariffin, S. H. S., Wong, K. Y., & Aun, Y. (2022). Indoor Positioning System: A Review. International Journal of Advanced Computer Science and Applications, 13(6), 477–490. doi:10.14569/IJACSA.2022.0130659.

[2] Cahyadi, M. N., & Rwabudandi, I. (2019). Integration of GNSS-IMU for increasing the observation accuracy in Condensed Areas (Infrastructure and Forest Canopies). E3S Web of Conferences, 94, 3015. doi:10.1051/e3sconf/20199403015.

[3] Cahyadi, M. N., Asfihani, T., Mardiyanto, R., & Erfianti, R. (2023). Performance of GPS and IMU sensor fusion using unscented Kalman filter for precise i-Boat navigation in infinite wide waters. Geodesy and Geodynamics, 14(3), 265–274. doi:10.1016/j.geog.2022.11.005.

[4] Cahyadi, M. N., Asfihani, T., Mardiyanto, R., & Erfianti, R. (2022). Loosely Coupled GNSS and IMU Integration for Accurate i-Boat Horizontal Navigation. International Journal of Geoinformatics, 18(3), 111–122. doi:10.52939/ijg.v18i3.2233.

[5] Meng, X., Wang, H., & Liu, B. (2017). A robust vehicle localization approach based on GNSS/IMU/DMI/LiDAR sensor fusion for autonomous vehicles. Sensors (Switzerland), 17(9), 2140. doi:10.3390/s17092140.

[6] Lin, J., Wang, R., Xiao, Z., Li, L., Yao, W., Han, W., & Zhao, B. (2017). Application of backpack Lidar to geological cross-section measurement. LIDAR Imaging Detection and Target Recognition 2017, 154. doi:10.1117/12.2295060.

[7] Aslinezhad, M., Malekijavan, A., & Abbasi, P. (2020). ANN-assisted robust GPS/INS information fusion to bridge GPS outage. Eurasip Journal on Wireless Communications and Networking, 2020(1), 129. doi:10.1186/s13638-020-01747-9.

[8] Cui, Y., Yang, B., Liu, P., & Kong, L. (2023). A Review of Indoor Automation Modeling Based on Light Detection and Ranging Point Clouds. Sensors and Materials, 35(1), 247. doi:10.18494/sam4211.

[9] Mousazadeh, H. (2013). A technical review on navigation systems of agricultural autonomous off-road vehicles. Journal of Terramechanics, 50(3), 211–232. doi:10.1016/j.jterra.2013.03.004.

[10] Strandberg, J., Hobiger, T., & Haas, R. (2019). Real-time sea-level monitoring using Kalman filtering of GNSS-R data. GPS Solutions, 23(3), 61. doi:10.1007/s10291-019-0851-1.

[11] Kaczmarek, A., Rohm, W., Klingbeil, L., & Tchórzewski, J. (2022). Experimental 2D extended Kalman filter sensor fusion for low-cost GNSS/IMU/Odometers precise positioning system. Measurement, 193, 110963. doi:10.1016/j.measurement.2022.110963.

[12] Tondaś, D., Ilieva, M., van Leijen, F., van der Marel, H., & Rohm, W. (2023). Kalman filter-based integration of GNSS and InSAR observations for local nonlinear strong deformations. Journal of Geodesy, 97(12), 109. doi:10.1007/s00190-023-01789-z.

[13] Hu, G., Xu, L., Gao, B., Chang, L., & Zhong, Y. (2023). Robust Unscented Kalman Filter-Based Decentralized Multisensor Information Fusion for INS/GNSS/CNS Integration in Hypersonic Vehicle Navigation. IEEE Transactions on Instrumentation and Measurement, 72, 1–11. doi:10.1109/TIM.2023.3281565.

[14] Falco, G., Pini, M., & Marucco, G. (2017). Loose and tight GNSS/INS integrations: Comparison of performance assessed in real Urban scenarios. Sensors (Switzerland), 17(2), 255. doi:10.3390/s17020255.

[15] Ryu, J. H., Gankhuyag, G., & Chong, K. T. (2016). Navigation System Heading and Position Accuracy Improvement through GPS and INS Data Fusion. Journal of Sensors, 7942963. doi:10.1155/2016/7942963.

[16] Yang, C., Shi, W., & Chen, W. (2018). Correlational inference-based adaptive unscented Kalman filter with application in GNSS/IMU-integrated navigation. GPS Solutions, 22(4), 100. doi:10.1007/s10291-018-0766-2.

[17] Li, X., Zhang, X., Niu, X., Wang, J., Pel, L., Yu, F., Zhang, H., Yang, C., Gao, Z., Zhang, Q., Zhu, F., Wen, W., Li, T., Liao, J., & Li, X. (2023). Progress and Achievements of Multi - sensor Fusion Navigation in China during 2019-2023. Journal of Geodesy and Geoinformation Science, 6(3), 102–114. doi:10.11947/j.JGGS.2023.0310.

[18] Navisa, S. C., Cahyadi, M. N., & Asfihani, T. (2023). Analysis of GNSS and IMU Sensor Data Fusion Using the Unscented Kalman Filter Method on Medical Drones in Open Air. IOP Conference Series: Earth and Environmental Science, 1250(1), 12019. doi:10.1088/1755-1315/1250/1/012019.

[19] Alaba, S. Y. (2024). GPS-IMU sensor fusion for reliable autonomous vehicle position estimation. arXiv (Preprint), 1-6. doi:10.48550/arXiv.2405.08119.

[20] Wang, Y., Xie, C., Liu, Y., Zhu, J., & Qin, J. (2024). A Multi-Sensor Fusion Underwater Localization Method Based on Unscented Kalman Filter on Manifolds. Sensors, 24(19), 6299. doi:10.3390/s24196299.

[21] Sun, D., Wei, M., Lyu, Y., Wang, D., Li, S., Li, W., He, L., & Zhu, S. (2024). A Gaussian Unscented Kalman Filter algorithm for indoor positioning system using Ultra Wide Band measurement. IET Radar, Sonar & Navigation, 19(1), 12682. doi:10.1049/rsn2.12682.

[22] Impraimakis, M., & Smyth, A. W. (2022). An unscented Kalman filter method for real time input-parameter-state estimation. Mechanical Systems and Signal Processing, 162, 108026. doi:10.1016/j.ymssp.2021.108026.

[23] Zhuang, Y., Sun, X., Li, Y., Huai, J., Hua, L., Yang, X., Cao, X., Zhang, P., Cao, Y., Qi, L., Yang, J., El-Bendary, N., El-Sheimy, N., Thompson, J., & Chen, R. (2023). Multi-sensor integrated navigation/positioning systems using data fusion: From analytics-based to learning-based approaches. Information Fusion, 95, 62–90. doi:10.1016/j.inffus.2023.01.025.

[24] Chen, H., & Sun, R. (2022). A GNSS Quality Control Based GNSS/IMU Integrated Navigation Algorithm in Urban Environments. China Satellite Navigation Conference (CSNC 2022) Proceedings. Lecture Notes in Electrical Engineering. Springer, Singapore. doi:10.1007/978-981-19-2588-7_40.

[25] Jiang, C., Zhao, D., Zhang, Q., & Liu, W. (2023). A Multi-GNSS/IMU Data Fusion Algorithm Based on the Mixed Norms for Land Vehicle Applications. Remote Sensing, 15(9), 2439. doi:10.3390/rs15092439.

[26] Shan, T., Englot, B., Meyers, D., Wang, W., Ratti, C., & Rus, D. (2020). LIO-SAM: Tightly-coupled Lidar Inertial Odometry via Smoothing and Mapping. 2020 IEEE/RSJ International Conference on Intelligent Robots and Systems (IROS), 5135–5142. doi:10.1109/iros45743.2020.9341176.

[27] Warku, H. T., Ko, N. Y., Yeom, H. G., & Choi, W. (2021). Three-Dimensional Mapping of Indoor and Outdoor Environment Using LIO-SAM. 2021 21st International Conference on Control, Automation and Systems (ICCAS), 1455–1458. doi:10.23919/iccas52745.2021.9649820.

[28] Triawan, L. A., Kurniawan, A., Raharjo, A. B., & Saptarini, D. (2024). Analysis of 3D Modeling Using LiDAR Velodyne for Tree Inventory Using the LIO-SAM Method. IOP Conference Series: Earth and Environmental Science, 1418(1), 12009. doi:10.1088/1755-1315/1418/1/012009.

[29] Cahyadi, M. N., Asfihani, T., Suhandri, H. F., & Erfianti, R. (2024). Unscented Kalman filter for a low-cost GNSS/IMU-based mobile mapping application under demanding conditions. Geodesy and Geodynamics, 15(2), 166–176. doi:10.1016/j.geog.2023.05.001.